Gömböc-Like Morphogenesis: Topological Constraints and Gradient-Driven Dynamics in Development

Arturo Tozzi *

Posted Date: 10 March 2026

doi: 10.20944/preprints202603.0795.v1

Keywords: robustness; canalization; attractor; morphodynamics; stability

 doi:10.20944/preprints202603.0795.v1

Article

Gömböc-Like Morphogenesis: Topological Constraints and Gradient-Driven Dynamics in Development

Arturo Tozzi

Via Comunale del Principe 13/a 80145, ASL Napoli 1 Centro, Distretto 27, Naples, Italy; tozziarturo@libero.it

Abstract

Developmental processes are usually described through dynamical systems and gradient-driven cellular rearrangements, yet their topological constraints are not well characterized. We introduce a mathematical approach linking morphogenesis with the Gömböc, a convex body whose equilibrium structure is minimal under topological constraints. We model developmental dynamics as gradient flows defined on a configuration space of tissue states where a morphogenetic potential integrates mechanical, chemical and adhesive cellular interactions. To explore how varying landscape parameters affect the stability of critical configurations and developmental trajectories, we simulated morphogenetic systems governed by gradient flows with Morse-type potentials. We found that systems approaching minimal critical-point structures display large basins of attraction and convergent trajectories despite diverse initial states. Developmental systems may operate near Gömböc-like dynamical regimes in which the topological properties of the configuration space constrain the number of accessible states, while attractors and gradient dynamics may induce a causal order. Our framework generates testable predictions. Developmental trajectories should concentrate into a small number of preferred channels, with transverse dispersion showing an exponential decay over time. In exponential morphogen gradients, migration time is expected to scale approximately linearly with the initial distance from the source. Saddle-like transitional configurations should appear as intermediate states in morphogenetic landscapes, detectable as brief phases of reduced migration speed and increased directional fluctuations. Overall, a quantitative framework is provided for analyzing developmental robustness, identifying transition bottlenecks in morphogenetic landscapes and predicting how physical or biochemical parameters could reshape developmental trajectories in synthetic and regenerative contexts.

Keywords: robustness; canalization; attractor; morphodynamics; stability

---

Introduction

The emergence of organized biological form from heterogeneous cellular assemblies is a cardinal problem in developmental biology. Classical explanations emphasize gene regulatory networks, biochemical gradients and mechanical interactions among cells, frequently modeled through reaction–diffusion systems, continuum tissue mechanics or agent-based simulations of cellular behavior (Kawasaki et al. 2018; Lee, Milinkovitch et al. 2023). These approaches have clarified the role of morphogens, adhesion forces and mechanical stresses in shaping developing tissues (Richtsmeier, and Kraft 2019; Gordon et al. 2020; Landge et al. 2020). Dynamical-systems frameworks have interpreted development as the progression of high-dimensional biological states governed by nonlinear interactions among biochemical and physical variables. Developmental trajectories are often represented as flows toward stable configurations in abstract landscapes defined by mechanical or biochemical potentials (Silbereis et al. 2016; Wagner and Klein 2020; Vivanco et al. 2024; López-

 doi:10.20944/preprints202603.0795.v1

Paleta, Moreno-Barbosa, and Velázquez-Castro 2025). However, most models focus on local interactions or parameterized networks without explicitly addressing how the topology of the configuration space constrains the number and arrangement of stable developmental outcomes. As a result, widely used concepts like canalization, attractor stability or developmental robustness are frequently invoked without explicit connection to the topological properties of the underlying dynamical system (Mojtahedi et al. 2016; Farrell et al. 2018; Francis and Swain 2018; Hota et al. 2022; Du et al. 2024; Majka et al. 2024). A more integrated perspective combining topology, causal ordering of developmental transitions and the geometry of dynamical landscapes could help clarify why biological systems repeatedly converge toward reproducible morphological configurations.

We introduce a framework explicitly linking morphogenesis to the concepts of Gömböc, topology and causality. The Gömböc is a geometric body characterized by the minimal equilibrium structure compatible with the topology of a convex surface, possessing a single stable and a single unstable equilibrium (Domokos, Papadopulos, and Ruina 1994; Várkonyi and Domokos 2006; Domokos and Várkonyi 2008; Chou and Friedman 2016). This property motivates the hypothesis that morphogenetic dynamics may operate in regimes where the number of critical configurations is constrained by topological structure. Therefore, we aim to model development as a gradient-driven process on a configuration space representing collective tissue states including spatial organization, mechanical tensions and chemical signaling fields. A morphogenetic potential integrates these interactions into a scalar landscape defined over the configuration space where the resulting dynamics follow the steepest descent. Within this framework, topology constrains the minimal number of critical configurations of the potential, while causality emerges from the directional structure of the gradient flow connecting unstable, transitional and stable states. To investigate these relationships, we implement numerical simulations of simplified morphogenetic systems governed by gradient dynamics with potentials constructed to approximate minimal critical-point structures analogous to the Gömböc equilibrium configuration. Our simulations explore how landscape geometry's modifications could affect the organization of developmental trajectories, the emergence of saddle-like transitional states and the convergence of diverse initial configurations toward stable morphological outcomes.

Our formulation leads to explicit, experimentally testable expectations concerning morphogenetic dynamics. Developmental trajectories are expected to concentrate into a limited number of preferred channels, while transverse dispersion should decrease approximately exponentially over time. In exponential morphogen gradients, migration time should scale roughly linearly with the initial distance from the source. Transitional configurations should correspond to saddle-like states in morphogenetic landscapes, appearing as brief phases characterized by reduced migration speed and increased directional fluctuations. Perturbations modifying landscape topology, like changes in morphogen gradients or tissue mechanical properties, should increase the number of stable configurations and broaden the range of attainable morphologies.

Methods

We studied Gömböc-like morphogenesis by simulating developmental gradient dynamics in a spatially extended tissue patch whose state is the position and orientation of migrating cells constrained by a morphogen field and a mechanical centering term. Computing trajectory ensembles and population time series as a function of chemotactic and mechanical parameters, we employed continuous-time gradient-flow formulation, numerical time integration and parameter sweeps to map how topology-compatible minimal attractor structure could shape convergence. We aimed to identify an experimentally discriminable signature defined as Gömböc-like global convergence, quantified by a large basin of attraction together with monotone decrease of a Lyapunov potential and sharply clustered convergence times across heterogeneous initial conditions.

Model state space and topology-compatible gradient structure. Cell configurations were represented by a state vector

$$z(t) = (x(t), y(t)) \in \Omega \subset \mathbb{R}^2$$

 doi:10.20944/preprints202603.0795.v1

where

$$\Omega = [0, L_x] \times [0, L_y]$$

is a planar tissue domain with

$$L_x = L_y = 1000\,\mu m.$$

Although the state is embedded in Euclidean space, the dynamical organization was analyzed through the induced causal reachability relation generated by a dissipative flow, which plays the role of an order structure on accessible states. Gömböc-like behavior was operationalized as a minimal attractor structure consisting of a single stable target region and the absence of recurrent orbits under the chosen dynamics.

The dynamical system was defined as a gradient-like flow driven by a scalar potential V such that

$$\frac{dV}{dt} \leq 0$$

along trajectories.

Specifically, a morphogen field $C(x)$ decreasing with distance from a source boundary was combined with a mechanical penalty attracting trajectories toward a preferred midline $y = y_0$. A Lyapunov candidate was constructed as

$$V(x, y) = \Phi(C(x)) + \frac{k_y}{2}(y - y_0)^2$$

where Φ is a monotonically decreasing function of C selected so that

$$\frac{\partial V}{\partial x}$$

aligns with the chemotactic drift direction.

The causality notion used in the analysis was induced by the flow map φ_t, defining

$$z \prec z' \text{ if } \exists t \geq 0 \text{ such that } z' = \varphi_t(z),$$

which is acyclic whenever V decreases strictly away from critical sets.

Morphogen field specification and units. The morphogen concentration was modeled as a one-dimensional boundary-driven profile that is uniform in y and decays in x, consistent with diffusion with effective degradation under steady-state conditions.

The field was defined in nanomolar units as

$$C(x) = C_0 e^{-x/\lambda}$$

with boundary concentration

$$C_0 = 100\,nM$$

at $x = 0$ and decay length

$$\lambda = 200\,\mu m.$$

The spatial derivative entering the chemotactic term was computed analytically:

$$\frac{dC}{dx}(x) = -\frac{C_0}{\lambda} e^{-x/\lambda}.$$

All spatial coordinates were measured in micrometers and time in hours. The tissue midline was set to

$$y_0 = 500\,\mu m.$$

Concentration evaluation used clamping

$$x \mapsto \min(\max(x, 0), L_x)$$

to prevent extrapolation outside the domain.

For visualization of the field, the domain was discretized on a regular grid

$$x_i \in [0, L_x], y_j \in [0, L_y]$$

with 201 points per axis and the scalar field $C(x_i)$ was replicated across $y$to obtain

$$C(x_i, y_j) = C(x_i).$$

 doi:10.20944/preprints202603.0795.v1

Gradient dynamics, saturation and Lyapunov monotonicity. Cell motion was modeled by chemotactic drift in x coupled to mechanical relaxation in y. The governing equations were

$$\frac{dx}{dt} = \chi \frac{dC/dx}{K + C(x)}$$

$$\frac{dy}{dt} = -k_y(y - y_0)$$

where χ is chemotactic sensitivity and k_y is a transverse relaxation rate.

Units were chosen so that

$$\chi\ [\mu m^2/(h \cdot nM)], \frac{dC}{dx}\ [nM/\mu m]$$

which gives

$$\frac{dx}{dt}\ [\mu m/h].$$

The Michaelis-type denominator

$$K + C(x)$$

with

$$K = 20\ nM$$

prevents unrealistically large drift near the source.

The mechanical term yields exponential relaxation

$$y(t) = y_0 + (y(0) - y_0)e^{-k_y t}.$$

A Lyapunov potential consistent with these dynamics can be written as

$$V(x, y) = \chi \log\,(K + C(x)) + \frac{k_y}{2}(y - y_0)^2.$$

Its gradients are

$$\frac{\partial V}{\partial x} = \chi \frac{C'(x)}{K + C(x)}$$

$$\frac{\partial V}{\partial y} = k_y(y - y_0).$$

Trajectories therefore satisfy monotone descent in V away from critical sets.

Morse-theoretic interpretation of critical configurations. The structure of critical configurations of the morphogenetic potential was interpreted using Morse theory (Zubov, Murygin, and Gerke 2022; Lipiński et al. 2023; Reani and Bobrowski 2026). Let

$$V: X \to \mathbb{R}$$

be the potential defined on the configuration space X. A function V is a Morse function when every critical point x^* satisfies

$$\nabla V(x^*) = 0$$

and the Hessian matrix

$$H_V(x^*) = \left[\frac{\partial^2 V}{\partial x_i\, \partial x_j}\right]$$

is non-degenerate:

$$\det\,(H_V(x^*)) \neq 0.$$

Each critical point is assigned a Morse index equal to the number of negative eigenvalues of the Hessian. In two dimensions: index 0 corresponds to minima; index 1 corresponds to saddle points; index 2 corresponds to maxima.

Morse theory relates the number of critical points to the topology of the configuration space through Morse inequalities linking these counts to Betti numbers.

 doi:10.20944/preprints202603.0795.v1

Our simulated potential was constructed to approximate a minimal configuration of critical points compatible with the topology of the state space. This minimal equilibrium arrangement is conceptually analogous to the Gömböc, characterized by the minimal equilibrium structure permitted by topology under gravitational dynamics (Figure 1). Dynamical systems approaching these minimal critical-point configurations tend to display large basins of attraction and strong convergence toward the stable state. In the morphogenetic context, this property suggests that developmental robustness may arise when the potential landscape contains only a small number of critical configurations. Under these conditions, a wide range of initial cellular states is directed toward the same morphological configuration, producing canalized developmental outcomes despite variability in initial conditions or perturbations. The Gömböc therefore could provide a geometric reference for minimal equilibrium organization in morphogenetic landscapes.

Numerical integration and ensemble design. Time integration used explicit Euler steps with step size

$$\Delta t = 0.01\,h$$

over a horizon

$$T = 20\,h.$$

The update equations were

$$x_{n+1} = x_n + \Delta t \chi \frac{C'(x_n)}{K + C(x_n)}$$

$$y_{n+1} = y_n - \Delta t k_y (y_n - y_0).$$

Initial conditions were sampled uniformly:

$$x(0) \sim U(300{,}950)\ \mu m$$

$$y(0) \sim U(100{,}900)\ \mu m.$$

Twenty-five trajectories were simulated per experiment.

Boundary conditions included clamping in x and reflection in y.

Flow-field visualization and induced causal organization. A vector field was computed on a grid restricted to

$$x \in [0{,}800]\ \mu m, y \in [200{,}800]\ \mu m.$$

Velocity components were

$$v_x(x_i, y_j) = \chi \frac{C'(x_i)}{K + C(x_i)}$$

$$v_y(x_i, y_j) = -k_y (y_j - y_0).$$

Streamplots of the resulting field visualize integral curves of the dynamical system and illustrate the basin structure of the attractor.

Convergence criterion, parameter sweep and reproducibility tools. Gömböc-like convergence was quantified using a hitting-time metric to a stable region

$$R = \{(x, y) \in \Omega : x \leq 100\ \mu m, |\ y - y_0\ | \leq 20\ \mu m\}.$$

The convergence time for each trajectory was

$$\tau = \inf\{t_n : (x_n, y_n) \in R\}.$$

A parameter sweep evaluated mean convergence times for

$$\chi \in [2000{,}14000]\ \mu m^2/(h \cdot nM)$$

$$k_y \in [0.1{,}1.2]\ h^{-1}$$

on a 9×9 grid.

For each parameter pair, twelve randomized initial states were simulated and the mean convergence time was computed.

All simulations were implemented in Python using NumPy for numerical computation and Matplotlib for visualization. A fixed pseudorandom seed ensured reproducibility of initial conditions and parameter sampling.

 doi:10.20944/preprints202603.0795.v1

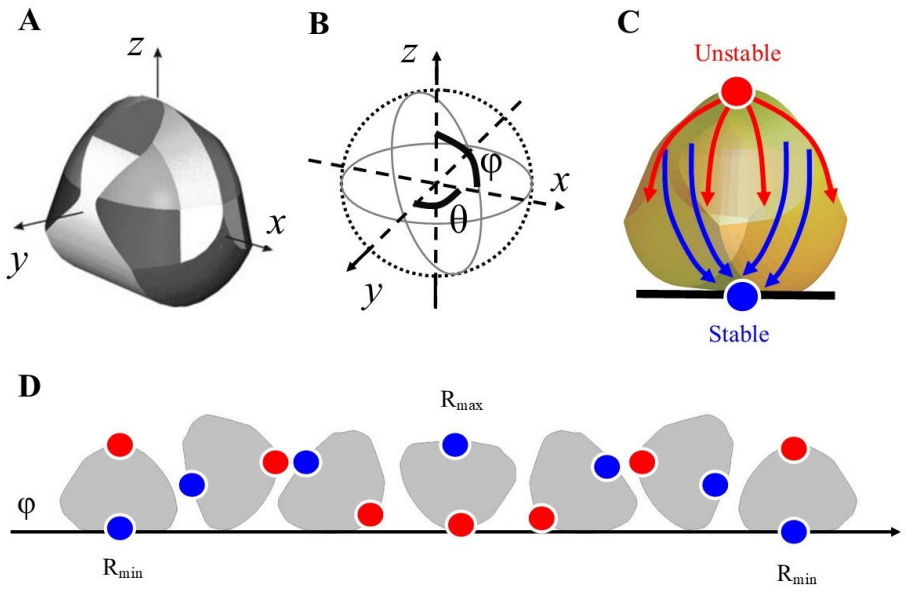

Figure 1. Geometry, orientation space and equilibrium structure of a Gömböc-like body. (A) A monostatic three-dimensional convex object (termed Gömböc) equipped with a single point of stable equilibrium, shown with Cartesian reference axes x, y, z defining the body orientation in space. (B) The Gömböc embedded in a spherical polar coordinate system centered at the center of gravity of the body, where three-dimensional shapes can be described by a radial function $R(\phi, \theta)$ that specifies the distance from the origin for each angular direction. (C) Schematic representation of the equilibrium structure of the Gömböc, which possesses exactly one stable equilibrium (blue point) and one unstable equilibrium (red point). Arrows represent trajectories of the gradient-like motion bringing the body toward the stable configuration. (D) Examples of feasible rolling paths of the Gömböc along a horizontal plane. Regardless of the initial orientation, the body evolves toward the single stable fixed point. $R_{\max}$ denotes the unstable equilibrium associated with the highest potential energy, whereas $R_{\min}$ denotes the stable equilibrium corresponding to the lowest energy. Modified from Domokos and Várkonyi (2008).

Results

We describe the dynamical organization of simulated morphogenetic trajectories generated by gradient-driven cell migration in a spatially extended tissue domain. Our analysis evaluates trajectory convergence, concentration sensing along trajectories and the parameter dependence of convergence times. Quantitative comparisons are based on the simulated ensemble of 25 trajectories evolving under identical dynamical rules but heterogeneous initial conditions.

Trajectory organization and concentration dynamics. Simulated trajectories exhibited coherent directional organization across the 1 mm by 1 mm domain, moving from heterogeneous starting positions toward a region near the morphogen source and mechanical midline (Figure 2). Initial positions were distributed uniformly within $x \in [300,950]\ \mu\text{m}$ and $y \in [100,900]\ \mu\text{m}$, yet the trajectories progressively aligned along a common dynamical channel defined by the chemotactic gradient and transverse relaxation. Among the 25 simulated cells, 8 trajectories entered the predefined convergence region $x \leq 100\ \mu\text{m}$ and $|y - 500| \leq 20\ \mu\text{m}$ within the 20-hour simulation window, corresponding to a convergence proportion of 0.32. For convergent trajectories, the mean convergence time was 13.58 h with a standard deviation of 4.04 h. Population-level sensing of the morphogen field increased monotonically along trajectories, as illustrated by the ensemble time series of sensed concentration (Figure 3). A paired statistical comparison between the initial and final concentrations sampled by each trajectory yielded a t-statistic of $t = 4.31$ with $p = 2.38 \times 10^{-4}$, indicating a systematic increase in sensed morphogen levels along the simulated developmental progression. The phase-flow representation confirmed that the vector field guiding motion displays a coherent directional structure with contraction toward the midline and drift toward the morphogen source (Figure 4).

 doi:10.20944/preprints202603.0795.v1

These results suggest that heterogeneous initial states evolve along ordered dynamical channels toward regions of lower potential under the imposed gradient dynamics, thereby providing the quantitative basis for examining convergence properties across parameter variations.

Parameter dependence and convergence structure. Variation of the chemotactic sensitivity and mechanical relaxation parameters showed systematic changes in the time required to reach the stable region (Figure 5). Across the ensemble used for convergence analysis, convergence time exhibited a strong dependence on the initial longitudinal position. The Pearson correlation coefficient between initial x-position and convergence time among trajectories that reached the stable region was $r = 0.998$ with $p < 0.001$, indicating that trajectories beginning further from the morphogen source required proportionally longer times to approach the convergence region. This dependence reflects the exponential decay of the morphogen gradient, which reduces chemotactic drift strength at larger distances. Heatmap analysis across the explored parameter grid demonstrated that increasing chemotactic sensitivity reduced convergence times, whereas stronger mechanical relaxation primarily influenced the vertical contraction rate without substantially altering longitudinal progression. Regions of parameter space combining high chemotactic sensitivity and moderate relaxation produced the shortest mean convergence times within the sampled parameter domain. These parameter-dependent differences were consistent with the structure of the velocity field, where the chemotactic term determines longitudinal acceleration while the mechanical term controls transverse stabilization.

Together, the statistical relationships between initial conditions, parameter values and convergence time define a structured dynamical landscape in which trajectory progression follows predictable gradients of the morphogenetic potential.

Overall, our results suggest that gradient-driven dynamics could generate organized morphogenetic trajectories characterized by monotonic increases in sensed morphogen concentration, directional phase flows and convergence toward spatially defined stable regions. Statistical analysis confirms that convergence timing is strongly determined by initial spatial position and the strength of the chemotactic drift. Therefore, topology-constrained gradient dynamics could produce organized developmental trajectories under heterogeneous initial conditions.

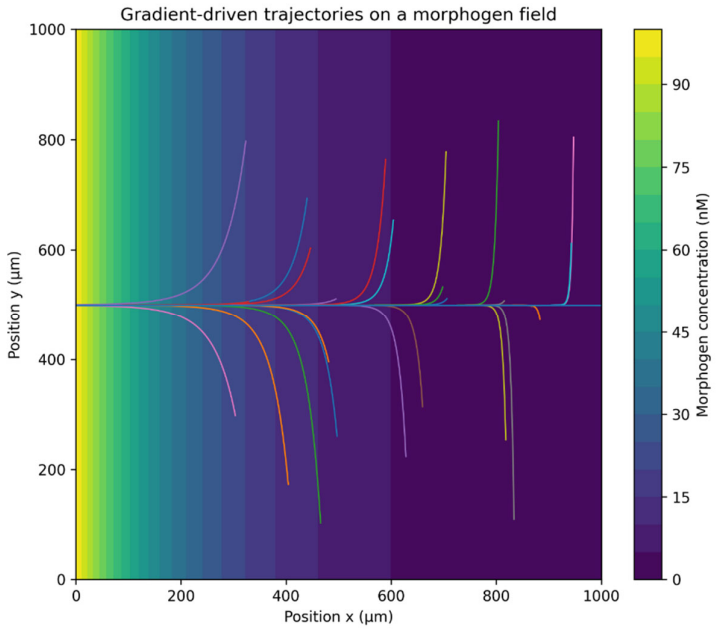

Figure 2. Simulated cell trajectories in a 1 mm by 1 mm tissue domain over a morphogen field with boundary concentration 100 nM and exponential decay length 200 μm. Cells undergo gradient dynamics with chemotactic sensitivity χ = 8000 μm² per hour per nM and mechanical relaxation toward a midline at y = 500 μm with rate k_γ

 doi:10.20944/preprints202603.0795.v1

= 0.5 per hour. Trajectories illustrate convergence toward a shared target region near the morphogen source, while remaining mechanically constrained in the transverse direction.

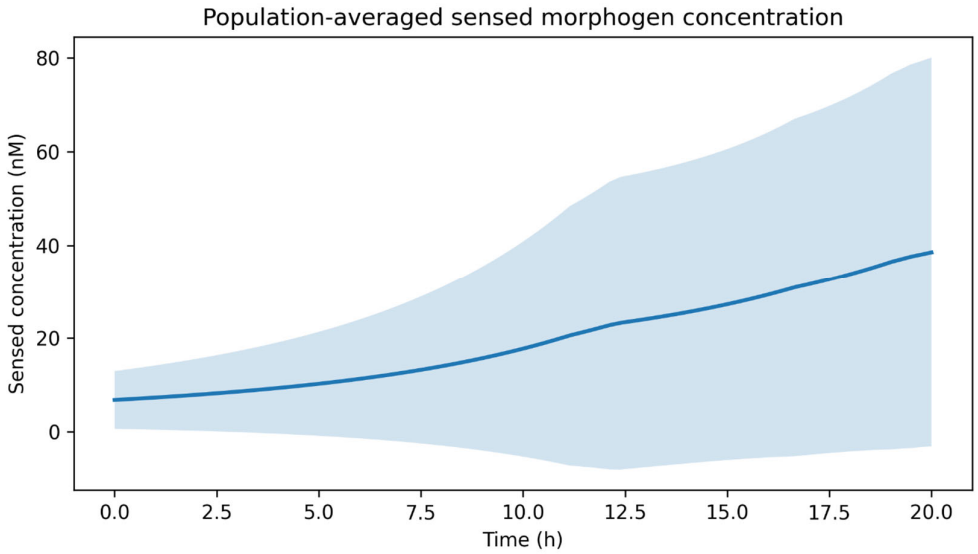

Figure 3. Population averaged sensed morphogen concentration during simulated migration plotted over 20 hours. The mean curve summarizes concentrations sampled along trajectories, with the shaded band indicating one standard deviation across cells. The monotone increase reflects gradient descent in the morphogenetic potential induced by chemotaxis, while dispersion quantifies sensitivity to initial condition variability under the same dynamic parameters and boundary conditions as the trajectory simulation.

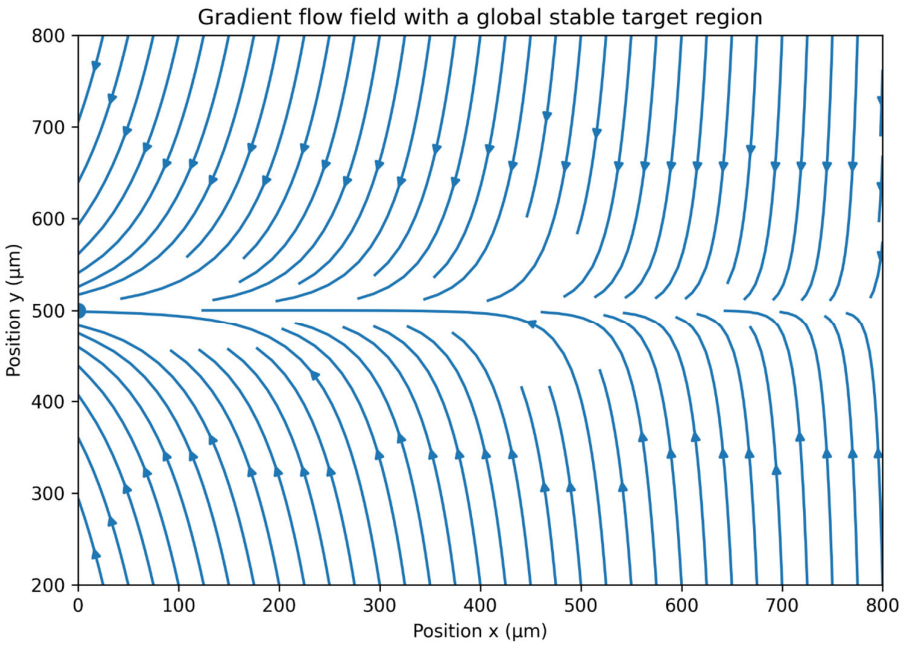

Figure 4. Streamplot of the induced gradient flow field in physical space, showing the directional structure that defines causality as reachability along trajectories. The horizontal component is driven by the morphogen gradient through a saturating chemotactic term, while the vertical component is a linear mechanical relaxation toward y = 500 μm. The marked point indicates the stable target line intersection near the source boundary, while streamlines visualize basin structure and the absence of cyclic transitions under a dissipative potential.

 doi:10.20944/preprints202603.0795.v1

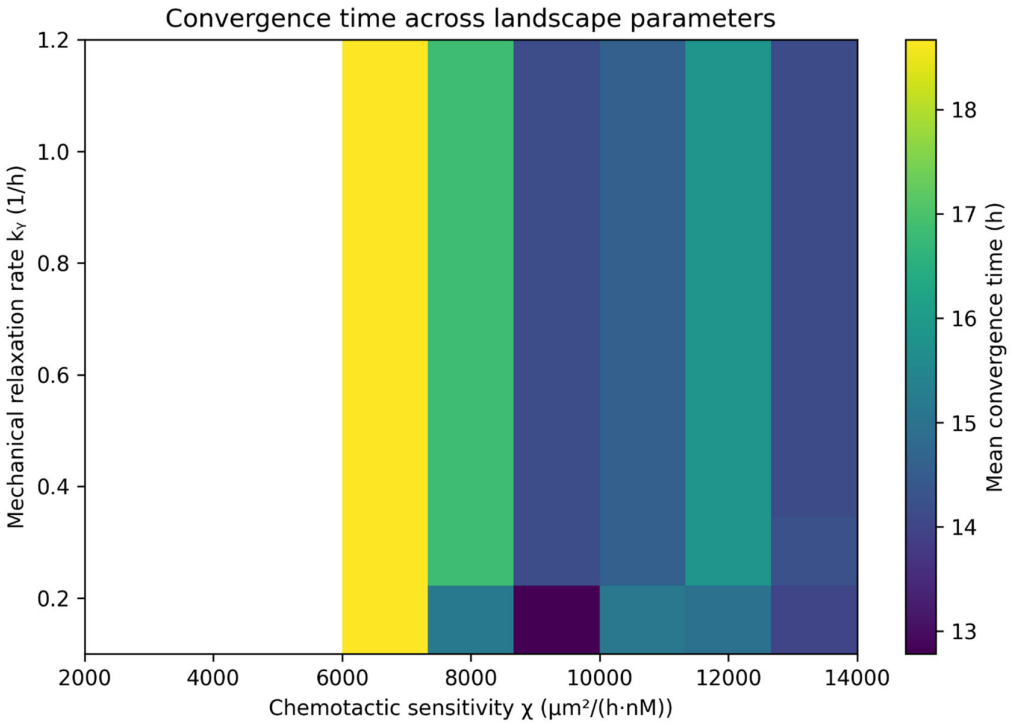

Figure 5. Mean convergence time to a predefined stable region ($x \leq 100$ μm and absolute deviation from $y = 500$ μm ≤ 20 μm) as a function of chemotactic sensitivity χ and mechanical relaxation rate k_γ. Each cell in the map averages convergence times over multiple randomized initial conditions within the domain. Parameter dependence quantifies how gradient dynamics and mechanical confinement jointly control the speed of convergence to a reproducible configuration.

Conclusions

We asked whether morphogenetic organization can be described as a gradient-driven dynamical process constrained by topological structure and whether these constraints can produce convergence patterns analogous to minimal equilibrium systems, including the geometric paradigm represented by the Gömböc. Our simulations compared ensembles of heterogeneous initial cellular configurations evolving under a morphogen gradient and mechanical relaxation toward a spatial midline. We examined trajectory organization, temporal changes in sensed morphogen concentration and the dependence of convergence behavior on dynamical parameters governing chemotactic sensitivity and transverse relaxation. We found that our simulated trajectories consistently reorganized along directed dynamical channels defined by the gradient field and mechanical constraint, producing monotonic increases in sensed morphogen concentration and structured flows toward spatially localized regions of lower potential. Convergence behavior varied quantitatively with the initial spatial distribution and with the strength of the chemotactic drift, while the relaxation term primarily stabilized transverse alignment. The resulting trajectories exhibited a coherent causal ordering in which developmental states were connected by a directed progression through configuration space. Therefore, morphogenetic dynamics can be represented as gradient flows constrained by the geometry of the state space and by the spatial structure of the morphogen field, with the Gömböc providing a conceptual reference for systems approaching minimal equilibrium structures.

Our model introduces an explicit link between equilibrium geometry and developmental dynamics by embedding morphogenetic trajectories within a potential high-dimensional landscape whose critical-point structure is constrained by topology. Existing developmental models describe pattern formation through local biochemical interactions or mechanical rules, but rarely quantify the

 doi:10.20944/preprints202603.0795.v1

global structure of the dynamical landscape governing state transitions. Our formulation, complementing Turing-like reaction–diffusion and mechanical models (Pickering and Towers 2016; Hiscock, Tschopp, and Tabin 2017; Cooper et al. 2018; Rolfe, Shea, and Murphy 2022; Kang et al. 2024), defines computable quantities like convergence time distributions, basin geometry of stable configurations and parameter-dependent trajectory organization.

Our study has limitations. The morphogen concentration profile, the chemotactic response function and the Lyapunov potential were not derived from experimentally measured biological parameters. The parameter values are plausible but not validated against specific developmental systems. The proposed Gömböc-like minimal critical structure is introduced conceptually, but the minimality of critical points is not formally proven. The interpretation of developmental trajectories in causal terms arises from the directed nature of the gradient flow and is therefore interpretative rather than formally demonstrated in a rigorous mathematical sense. All figures originate from a simplified numerical model and are not calibrated against experimental datasets. Additional work is needed to incorporate stochastic fluctuations, cell proliferation and mechanical feedback between cells and the extracellular matrix.

Experimentally testable hypotheses arise from our simulated dynamics.

1. First, gradient-driven morphogenetic systems should exhibit trajectory clustering in configuration space. Time-resolved imaging of migrating cells exposed to controlled morphogen gradients should reveal that trajectories converge into a limited number of dynamical channels rather than spreading uniformly across the tissue. Quantitatively, the dispersion of trajectories perpendicular to the dominant migration direction is expected to decrease over time approximately as

$$\sigma_y(t) \approx \sigma_y(0)e^{-k_y t},$$

where k_y represents the effective transverse relaxation rate measurable from tracking data.

2. Second, convergence time should scale with initial distance from the morphogen source. In systems where morphogen concentration follows an exponential spatial profile $C(x) = C_0 e^{-x/\lambda}$, the expected time required for cells to reach a threshold concentration region should increase approximately linearly with the initial distance when chemotactic drift dominates diffusion. Empirical measurements of migration time versus starting position could test this scaling relation and estimate effective chemotactic sensitivity.
3. Third, transitional configurations should correspond to saddle-like regions in the morphogenetic landscape. In live-imaging experiments, these states would appear as transient spatial arrangements where migration velocity decreases and directional fluctuations increase before trajectories reorganize toward stable configurations.

Previous work in developmental and cell migration biology provides partial support for several aspects of these predictions. Directional alignment of migrating cells along morphogen or chemotactic gradients has been documented in systems like *Dictyostelium* aggregation, neural crest migration and epithelial collective migration, where cells organize into streams or dynamically aligned trajectories rather than dispersing randomly across tissues (Rørth 2012; Shellard and Mayor 2016; Tweedy, Knecht, Mackay and Insall 2016). Quantitative analyses of chemotaxis evaluate mean velocity, chemotactic index or persistence time, but rarely examine the temporal contraction of transverse trajectory dispersion predicted by relaxation dynamics. Similarly, theoretical chemotaxis models based on Keller–Segel–type equations and later refinements predict that migration speed depends on morphogen gradient strength, implying that cells located further from the source experience weaker drift and longer travel times (Keller and Segel 1971; Painter 2009). However, our explicit tests of simple scaling relations between initial distance and arrival time are uncommon. Dynamical-systems interpretations of developmental processes describe differentiation and morphogenetic transitions in terms of motion on potential-like landscapes, where stable

 doi:10.20944/preprints202603.0795.v1

configurations correspond to attractors and transitional states may resemble saddle points separating alternative trajectories (Ferrell 2012; Huang 2010). These studies support the qualitative plausibility of our predictions, while leaving our specific quantitative suggestions largely unexplored.

In experimental settings under controlled perturbations, our approach could support the interpretation of high-resolution imaging datasets by providing mathematical descriptors of collective cellular motion and spatial reorganization. Measurements of trajectory distributions, migration velocities and spatial contraction rates could be integrated into computational pipelines to estimate the parameters governing tissue-scale dynamics. Our approach also provides a way to compare distinct developmental conditions such as altered morphogen production or modified tissue stiffness, by mapping how parameter changes reorganize the set of accessible configurations. In engineered biological systems, numerical exploration of dynamical landscapes could assist the identification of parameter regimes that generate reproducible structural outcomes.

In conclusion, we investigated how spatial organization can arise from directed dynamical evolution in a simulated tissue environment governed by a morphogen field and mechanical constraint. We provided numerical simulations to explore trajectory organization, temporal progression of state variables and parameter-dependent convergence behavior across heterogeneous initial conditions. We concluded that structured dynamical landscapes can generate orderly developmental progressions, providing a mathematical description of how spatial configurations evolve toward stable states within controlled simulation conditions.

Author Contributions: The Author performed: study concept and design, acquisition of data, analysis and interpretation of data, drafting of the manuscript, critical revision of the manuscript for important intellectual content, statistical analysis, obtained funding, administrative, technical and material support, study supervision.

Funding: This research did not receive any specific grant from funding agencies in the public, commercial or not-for-profit sectors.

Informed Consent Statement: The Author transfers all copyright ownership, in the event the work is published. The undersigned author warrants that the article is original, does not infringe on any copyright or other proprietary right of any third part, is not under consideration by another journal and has not been previously published.

Data Availability Statement: All data and materials generated or analyzed during this study are included in the manuscript. The Author had full access to all the data in the study and took responsibility for the integrity of the data and the accuracy of the data analysis.

Conflicts of Interest: The Author does not have any known or potential conflict of interest including any financial, personal or other relationships with other people or organizations within three years of beginning the submitted work that could inappropriately influence or be perceived to influence their work.

Ethics Approval and Consent to Participate: This research does not contain any studies with human participants or animals performed by the Author.

Declaration: of generative AI and AI-assisted technologies in the writing process. During the preparation of this work, the author used ChatGPT 5.2 to assist with data analysis and manuscript drafting and to improve spelling, grammar and general editing. After using this tool, the author reviewed and edited the content as needed, taking full responsibility for the content of the publication.

References

Chou, Ching-Shan, and Avner Friedman. 2016. “System of Two Linear Differential Equations.” In *Introduction to Mathematical Biology*, 29–42. New York: Springer.

Cooper, R. L., A. P. Thiery, A. G. Fletcher, D. J. Delbarre, L. J. Rasch, and G. J. Fraser. 2018. “An Ancient Turing-Like Patterning Mechanism Regulates Skin Denticle Development in Sharks.” *Science Advances* 4 (11): eaau5484. https://doi.org/10.1126/sciadv.aau5484.

 doi:10.20944/preprints202603.0795.v1

Domokos, Gábor, J. Papadopulos, and Andy Ruina. 1994. "Static Equilibria of Planar, Rigid Bodies: Is There Anything New?" *Journal of Elasticity* 36: 59–66.

Domokos, Gábor, and Péter L. Várkonyi. 2008. "Geometry and Self-Righting of Turtles." *Proceedings of the Royal Society B: Biological Sciences* 275: 11–17. https://doi.org/10.1098/rspb.2007.1188.

Du, J., Y. Liu, J. Sun, E. Yao, J. Xu, X. Wu, L. Xu, M. Zhou, G. Yang, and X. Jiang. 2024. "ARID1A Safeguards the Canalization of the Cell Fate Decision during Osteoclastogenesis." *Nature Communications* 15 (1): 5994. https://doi.org/10.1038/s41467-024-50225-z.

Farrell, J. A., Y. Wang, S. J. Riesenfeld, K. Shekhar, A. Regev, and A. F. Schier. 2018. "Single-Cell Reconstruction of Developmental Trajectories during Zebrafish Embryogenesis." *Science* 360 (6392): eaar3131. https://doi.org/10.1126/science.aar3131.

Ferrell, James E., Jr. 2012. "Bistability, Bifurcations and Waddington's Epigenetic Landscape." *Current Biology* 22 (11): R458–R466.

Francis, J. C., and A. Swain. 2018. "Prostate Organogenesis." *Cold Spring Harbor Perspectives in Medicine* 8 (7): a030353. https://doi.org/10.1101/cshperspect.a030353.

Gordon, N. K., Z. Chen, R. Gordon, and Y. Zou. 2020. "French Flag Gradients and Turing Reaction-Diffusion versus Differentiation Waves as Models of Morphogenesis." *Biosystems* 196: 104169. https://doi.org/10.1016/j.biosystems.2020.104169.

Hiscock, T. W., P. Tschopp, and C. J. Tabin. 2017. "On the Formation of Digits and Joints during Limb Development." *Developmental Cell* 41 (5): 459–465. https://doi.org/10.1016/j.devcel.2017.04.021.

Hota, S. K., K. S. Rao, A. P. Blair, A. Khalilimeybodi, K. M. Hu, R. Thomas, K. So, V. Kameswaran, J. Xu, B. J. Polacco, et al. 2022. "Brahma Safeguards Canalization of Cardiac Mesoderm Differentiation." *Nature* 602 (7895): 129–134. https://doi.org/10.1038/s41586-021-04336-y.

Huang, S. 2010. "Cell Lineage Determination in State Space: A Systems View Brings Flexibility to Dogmatic Canonical Rules." *PLoS Biology* 8 (5): e1000380. https://doi.org/10.1371/journal.pbio.1000380.

Kang, T. Y., F. Bocci, Q. Nie, J. N. Onuchic, and A. Levchenko. 2024. "Spatial-Temporal Order-Disorder Transition in Angiogenic NOTCH Signaling Controls Cell Fate Specification." *eLife* 12: RP89262. https://doi.org/10.7554/eLife.89262.

Kawasaki, M., K. Kawasaki, F. Meguro, A. Yamada, R. Ishikawa, et al. "Lrp4/Wise Regulates Palatal Rugae Development through Turing-Type Reaction-Diffusion Mechanisms." *PLoS ONE* 13 (9): e0204126. https://doi.org/10.1371/journal.pone.0204126.

Keller, Evelyn F., and Lee A. Segel. 1971. "Model for Chemotaxis." *Journal of Theoretical Biology* 30 (2): 225–234.

Landge, Aditya N., B. M. Jordan, X. Diego, and P. Müller. 2020. "Pattern Formation Mechanisms of Self-Organizing Reaction-Diffusion Systems." *Developmental Biology* 460 (1): 2–11. https://doi.org/10.1016/j.ydbio.2019.10.031.

Lee, C., J. T. Richtsmeier, and R. H. Kraft. 2019. "A Coupled Reaction-Diffusion-Strain Model Predicts Cranial Vault Formation in Development and Disease." *Biomechanics and Modeling in Mechanobiology* 18 (4): 1197–1211. https://doi.org/10.1007/s10237-019-01139-z.

Lipiński, Michał, Jakub Kubica, Marian Mrozek, and Thomas Wanner. 2023. "Conley–Morse–Forman Theory for Generalized Combinatorial Multivector Fields on Finite Topological Spaces." *Journal of Applied and Computational Topology* 7 (2): 139–184. https://doi.org/10.1007/s41468-022-00102-9.

López-Paleta, N., E. Moreno-Barbosa, and J. Velázquez-Castro. 2025. "A Fast Validation Test of Gene Regulatory Network Models via the Fokker–Planck Equation." *Journal of Biological Physics* 51 (1): 16. https://doi.org/10.1007/s10867-025-09681-x.

Majka, M., N. B. Becker, P. R. Ten Wolde, M. Zagorski, and T. R. Sokolowski. 2024. "Stable Developmental Patterns of Gene Expression without Morphogen Gradients." *PLoS Computational Biology* 20 (12): e1012555. https://doi.org/10.1371/journal.pcbi.1012555.

Milinkovitch, Michel C., E. Jahanbakhsh, and S. Zakany. 2023. "The Unreasonable Effectiveness of Reaction Diffusion in Vertebrate Skin Color Patterning." *Annual Review of Cell and Developmental Biology* 39: 145–174. https://doi.org/10.1146/annurev-cellbio-120319-024414.

 doi:10.20944/preprints202603.0795.v1

Mojtahedi, M., A. Skupin, J. Zhou, I. G. Castaño, R. Y. Leong-Quong, H. Chang, K. Trachana, A. Giuliani, and S. Huang. 2016. "Cell Fate Decision as High-Dimensional Critical State Transition." *PLoS Biology* 14 (12): e2000640. https://doi.org/10.1371/journal.pbio.2000640.

Painter, Kevin J. 2009. "Continuous Models for Cell Migration in Tissues and Applications to Cell Sorting via Differential Chemotaxis." *Bulletin of Mathematical Biology* 71 (5): 1117–1147.

Pickering, J., and M. Towers. 2016. "Inhibition of Shh Signalling in the Chick Wing Gives Insights into Digit Patterning and Evolution." *Development* 143 (19): 3514–3521. https://doi.org/10.1242/dev.137398.

Reani, Yossi, and Omer Bobrowski. 2026. "Morse Theory for the k-NN Distance Function." *Discrete & Computational Geometry* 75 (2): 491–510. https://doi.org/10.1007/s00454-025-00795-6.

Rolfe, R. A., C. A. Shea, and P. Murphy. 2022. "Geometric Analysis of Chondrogenic Self-Organisation of Embryonic Limb Bud Cells in Micromass Culture." *Cell and Tissue Research* 388 (1): 49–62. https://doi.org/10.1007/s00441-021-03564-y.

Rørth, Pernille. 2012. "Fellow Travellers: Emergent Properties of Collective Cell Migration." *EMBO Reports* 13 (11): 984–991.

Shellard, Adam, and Roberto Mayor. 2016. "Chemotaxis during Neural Crest Migration." *Seminars in Cell & Developmental Biology* 55: 111–118.

Silbereis, John C., Sushmita Pochareddy, Yao Zhu, Mingfeng Li, and Nenad Sestan. 2016. "The Cellular and Molecular Landscapes of the Developing Human Central Nervous System." *Neuron* 89 (2): 248–268. https://doi.org/10.1016/j.neuron.2015.12.008.

Tweedy, Luke, David A. Knecht, Gary M. Mackay, and Robert H. Insall. 2016. "Self-Generated Chemoattractant Gradients: Attractant Depletion Extends the Range and Robustness of Chemotaxis." *Cell* 167 (2): 1–13.

Vivanco, E., E. Goles, M. Montalva-Medel, and M. J. Poupin. 2024. "Dynamical Robustness of a Boolean Model for the Human Gonadal Sex Determination." *Computational Biology and Chemistry* 113: 108225. https://doi.org/10.1016/j.compbiolchem.2024.108225.

Várkonyi, Péter L., and Gábor Domokos. 2006. "Static Equilibria of Rigid Bodies: Dice, Pebbles, and the Poincaré–Hopf Theorem." *Journal of Nonlinear Science* 16: 255–281.

Wagner, Daniel E., and Allon M. Klein. 2020. "Lineage Tracing Meets Single-Cell Omics: Opportunities and Challenges." *Nature Reviews Genetics* 21 (7): 410–427. https://doi.org/10.1038/s41576-020-0223-2.

Zubov, A. S., D. A. Murygin, and K. M. Gerke. 2022. "Pore-Network Extraction Using Discrete Morse Theory: Preserving the Topology of the Pore Space." *Physical Review E* 106 (5–2): 055304. https://doi.org/10.1103/PhysRevE.106.055304.